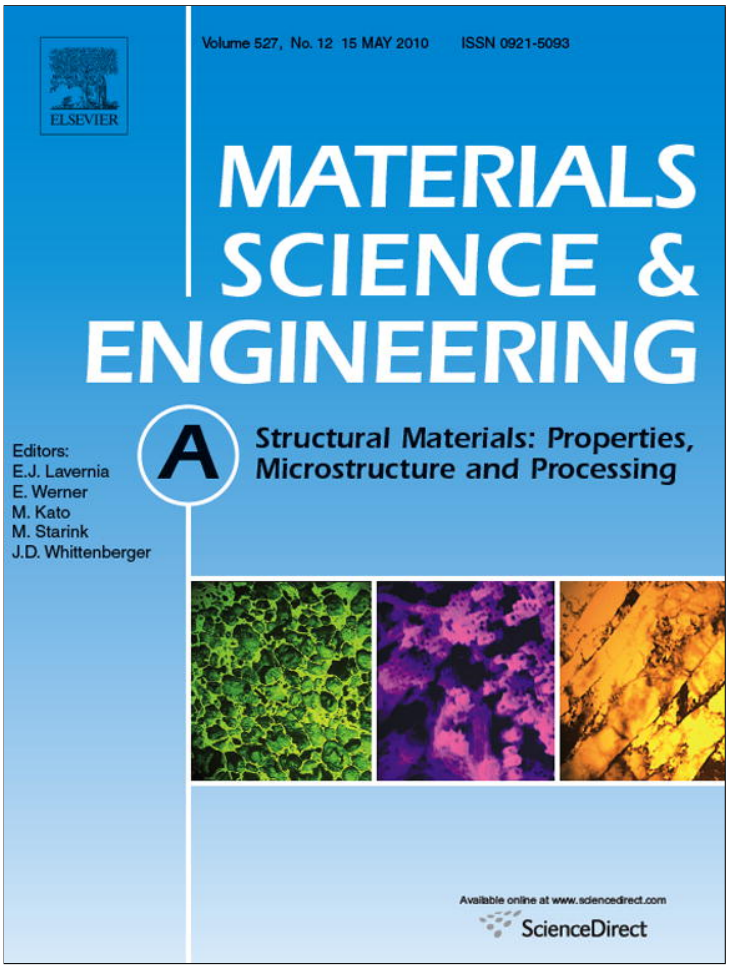

Materials Science and Engineering A 527 (2010) 2845–2856

Contents lists available at ScienceDirect

Materials Science and Engineering A

journal homepage: www.elsevier.com/locate/msea

Quasi-static and dynamic compression response of a lightweight interpenetrating phase composite foam

C. Periasamy, R. Jhaver, H.V. Tippur*

Department of Mechanical Engineering, Auburn University, 270 Ross Hall, Auburn, AL 36849, United States

ARTICLE INFO

Article history:
Received 15 September 2009
Received in revised form
29 December 2009
Accepted 21 January 2010

Keywords:
Compression response
Structural foams
Syntactic foam
Interpenetrating networks
Strain-rate effects

ABSTRACT

Quasi-static and dynamic compression response of syntactic foam (SF)–aluminum foam interpenetrating phase composites (IPC) is examined. Infusion of uncured syntactic foam (epoxy filled with hollow microballoons) into an open-cell aluminum network results in a 3D interpenetrating structure upon curing. The compression responses are measured at strain rates of ~0.001/s and 1500/s. The dynamic experiments are performed using a split Hopkinson pressure bar set up. The role of volume fraction of microballoons on the response of IPC is examined in terms of yield stress, plateau stress and energy absorption under quasi-static and dynamic conditions. The response of IPC samples are also compared with those made using syntactic foam alone. The results show that the energy absorbed by the IPC foams under dynamic loading is consistently higher than that measured under quasi-static loading conditions. For all volume fractions of microballoons, the IPC samples have better compression characteristics when compared to the corresponding syntactic foam samples. The failure modes and mechanisms of SF and IPC foams are examined both optically (using high-speed photography) and microscopically and the underlying differences are discussed.

1. Introduction

Multifunctional materials that are lightweight, stiff, strong and tough are of interest to many engineering disciplines for civil and military applications. In this context, a new class of materials called interpenetrating phase composites (IPC) has received attention in recent years [1]. IPCs are multiphase materials in which each constituent forms a continuous 3D network within the material volume. Thus, each phase in its stand alone state has an open-cell microstructure. Furthermore, even though IPCs are heterogeneous on a micro/meso scale, the macroscale response is often isotropic. This co-existence of desirable properties without significant directional dependency or distinct weak planes makes an IPC attractive for structural applications. For example, one phase might offer good toughness and thermal conductivity, while the other phase might enhance stiffness and dielectric properties. Thus, each phase of an IPC contributes its unique property to the overall structural response synergistically.

Among the existing works on IPCs, Prielipp et al. [2] studied the mechanical properties of aluminum/alumina interpenetrating composite and measured fracture strength and fracture toughness of the composite as a function of ligament diameter and volume fraction of the metal reinforcement. The metal reinforced interpenetrating composites consistently had higher fracture strength. Breslin et al. [3] characterized an aluminum/alumina IPC using the method of liquid phase displacement reaction method. The resulting IPC had enhanced density, thermal conductivity and CTE characteristics, without compromising stiffness or fracture toughness. Travitzky et al. [4] showed that the residual stresses developed in silicon during solidification of molten Si within an Al_2O_3 matrix results in better strength and fracture toughness of the resulting Al_2O_3/Si interpenetrating system. Wegner and Gibson [5] developed finite element models to predict the elastic, flow and thermal expansion properties of two phase IPCs. They attributed the enhancement in the thermo-mechanical properties to the contiguity of the phase with the most desirable property. In a later work [6], Wegner and Gibson studied the mechanical behavior of resin-impregnated porous stainless steel. The yield strength, ultimate strength, elongation at failure and the elastic modulus were all found to increase with an increasing volume fraction of steel. Skirl et al. [7] examined the thermal expansion behavior of alumina/aluminum IPC. A pressure infiltration technique was used to introduce aluminum into slip cast and then sintered alumina. The tensile and compressive residual stresses in alumina and aluminum phases were found to enhance the overall thermal coefficient of expansion. An increase in failure strain with increase in the metal content was also reported. Mayer and Papakyriacou [8] studied the fatigue behavior of graphite/aluminum IPC. The lightweight metals such as aluminum were infiltrated into polycrystalline graphite

* Corresponding author. Fax: +1 334 844 3327.
E-mail address: htippur@eng.auburn.edu (H.V. Tippur).

0921-5093/$ – see front matter © 2010 Elsevier B.V. All rights reserved.
doi:10.1016/j.msea.2010.01.066

to improve the fracture toughness of polycrystalline graphite. A 30% increase in the cyclic strength and a 10% increase in the endurance limit were reported. Tilbrook et al. [9] measured the effective mechanical properties of alumina-epoxy interpenetrating composites and reported strong dependence of properties on the composition and the processing of the material itself. The flexural strength and fracture toughness of graphite/aluminum IPC at room temperature and at 300 °C were examined by Etter et al. [10]. A 200% improvement in both these characteristics for IPC over un-infiltrated material at room temperature was reported. Also, no significant drop in properties was seen at elevated temperatures. Jhaver and Tippur [11] demonstrated the feasibility of a lightweight IPC foam by infiltrating a syntactic foam (SF) [12–14] into an open-cell aluminum network and examined quasi-static uniaxial compression response experimentally and numerically.

As noted in the above reports, the enhancements in the effective mechanical properties of IPC are dictated by the contiguity of the phase with the most desirable properties. Based on this, and pinning on the necessity to enhance the compression characteristics of structural foams, in this paper a lightweight IPC formed by infiltrating syntactic foam[1] (SF) into open-cell aluminum network is proposed for static as well as dynamic applications. An IPC foam formed by continuous interpenetrating 3D network of syntactic and aluminum foams has the potential for improving the structural integrity with good energy absorption characteristics, thus making it a worthwhile material system to study further. The present work builds on the feasibility study of the IPC foam first reported in Ref. [11]. In the current work, the performance of the material system and its mechanical behaviors are studied under both static and dynamic compression. The quasi-static mechanical responses are compared with the dynamic ones obtained using a split Hopkinson pressure bar measurements. High-speed photography and microstructural observations are used to distinguish failure mechanisms of SF and IPC materials. In the next section of this paper, the SF and IPC material preparation details are discussed. In Section 3, the experimental methods used are elaborated. Sections 4 and 5 present the effect of microballoon volume fraction on the quasi-static and dynamic compressive responses of SF and IPC, respectively. Section 6 of this paper discusses and compares the energy absorption characteristics under quasi-static and dynamic loading conditions. The progression of failure is analyzed photographically in Section 7. The results of the study are summarized in Section 8.

2. Material and specimen preparation

The constituents used for preparing the IPC foam were a low viscosity epoxy (Epo-Thin™ from Beuhler, Inc. USA, mass density of resin ~1100 kg/m^3), hollow glass microballoons (K-1™ microballoons from 3M Corp., bulk density 125 kg/m^3) of average diameter of ~60 μm and wall thickness of ~0.6 μm and commercially available open-cell Duocel® aluminum (Al6101-T6) foam obtained from ERG aerospace Corp., with a pore density of 40 pores per inch (~8% relative density). The above-mentioned material properties were provided by the respective manufacturers. The metal foam was cleaned and then coated with silane, γ-aminopropyltrimethoxysilane ($H_2NC_2H_4NHC_3H_6Si(OCH_3)_3$) to enhance the bond strength between the aluminum ligaments and the syntactic foam. Syntactic foam was then prepared by mixing the desired quantity of microballoons into epoxy resin. The uncured syntactic foam was then transferred into a silicone rubber mold after vacuuming (at approximately −75 kPa gage pressure) to remove any trapped air bubbles in the mixture. In case an IPC was desired, the silane coated aluminum foam was slowly inserted into the mold containing the uncured syntactic foam so that the syntactic foam fills in the open-pores of the aluminum network. After curing for at least seven days, the unfinished sample was removed from the mold for machining. A photograph of the cross-section of the cured IPC foam is shown in Fig. 1(a). The shiny metallic ligaments of the aluminum preform interspersed within the SF foam can be readily observed.

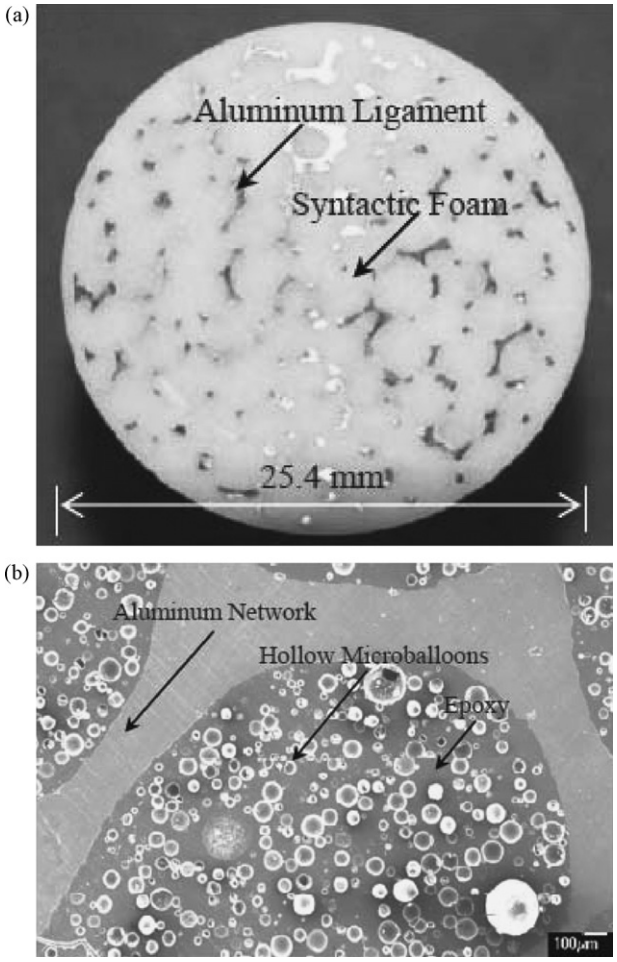

Fig. 1. (a) Cross-section of IPC foam with 30% volume fraction of SF and (b) SEM micrograph of IPC.

The cylindrical specimens used in quasi-static testing were 20 mm thick and 26.7 mm in diameter. These specimen dimensions were chosen in order to maintain the length to diameter (l/d) ratio less than 1. A higher l/d ratio has been shown to have significant effect in the compressive strength of syntactic epoxy foams by Song et al. [16]. The samples used in dynamic testing had a length of 9.5 mm and a diameter of 12.7 mm. Gibson [17] has proposed a specimen length to cell size ratio (l/D) of 8 or above, so that the specimen represents the bulk of the foam. The aluminum foam used in this work had a pore density of ~40 pores per inch with individual cell size of approximately 0.025 in. (0.635 mm). To be conservative, an l/D ratio of 15 was used in the current work. Fig. 1(b) shows a micrograph of the cross-section of the IPC with 30% microballoon volume fraction in SF. The interface between the

[1] Syntactic foams (SF) are structural foams with closed-cell structure made by dispersing *hollow* microballoons in a matrix to achieve lightweight characteristics. Typically they are made by dispersing thin-walled glass microballoons in a polymer matrix [13–16]. They are used by the electronic industry for their good dielectric properties [14], by the gas distribution industry for thermal insulation and in naval and aerospace applications for their excellent buoyancy and energy absorption characteristics, respectively [12,14,16]. Due to its multifunctionality SF is a worthwhile material to study as well.

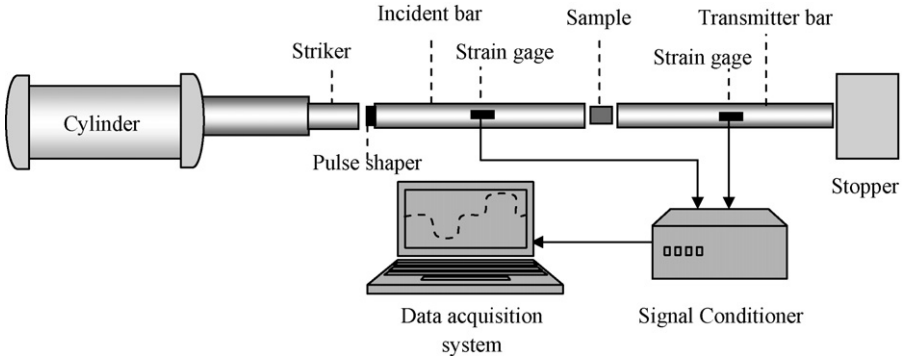

Fig. 2. Schematic of compression split Hopkinson pressure bar setup.

aluminum ligaments and the syntactic foam is well defined without voids or cracks suggesting a good bond between the aluminum and SF phases. The microballoons also appear to be randomly and uniformly distributed within the epoxy matrix.

3. Experimental details

3.1. Quasi-static experiments

The quasi-static uniaxial compression experiments were conducted according to ASTM standard D-695 for plastics and at room temperature using a MTS universal testing machine fitted with a 100 kN load cell. The two parallel faces of the samples were coated with graphite powder or grease for lubrication between the sample and the platens. The two lubricants gave a very similar load-deflection response and hence grease was used in all the subsequent experiments. The tests were performed under displacement controlled conditions with a cross-head speed of 1.25 mm/min. At least three samples of each volume fraction were tested to check for repeatability [11].

3.2. Dynamic experiments

The dynamic experiments were performed using a split Hopkinson pressure bar (SHPB) [18] apparatus developed for this study. The SHPB (Fig. 2) consisted of an air pressure cylinder, a striker (25.4 mm diameter and 406 mm long) held inside a barrel that is connected to the cylinder, a pulse shaper, an incident bar (25.4 mm diameter and 2438 mm long), a transmitter bar (25.4 mm diameter and 2438 mm long), a stopper, two strain gages (one on each bar), a signal conditioning unit and a data acquisition system. Both the striker and the two bars were made of Al-7075 of the same diameter in order to eliminate the impedance mismatch between them. The sample was held snug in between the incident and the transmitter bars prior to loading. The sample ends were coated with a thin layer of grease to position the sample and minimize friction at the interfaces. A pulse shaper [23], a 6.4 mm diameter disc made of a stack of four sheets of adhesively backed copper tapes each 0.1 mm thick, was used at the front end of the incident bar. The interface between the pulse shaper and the incident bar was also coated with grease for tackiness. The use of pulse shaper helped to achieve dynamic stress equilibrium in the sample for the loading duration. The strain histories on the bars were captured by the two strain gages mounted on the incident and the transmitter bars, and recorded as voltage histories in the data acquisition system (LeCroy^{TM} high-speed digital oscilloscope) after being processed by a signal conditioning unit (Ectron^{TM} transducer – signal conditioning amplifier). The oscilloscope acquired the strain signals at a rate of 2.5×10^6 samples per second as voltage histories. These voltage histories were then used to calculate the strain histories on the bars.

The stress $\sigma(t)$, strain rate $\dot{\varepsilon}(t)$ and strain $\varepsilon(t)$ histories of the sample were calculated using split Hopkinson bar equations [19] below:

$$\sigma(t) = E_0 \frac{A_0}{A} \varepsilon_T(t) \tag{1}$$

$$\dot{\varepsilon}(t) = -\frac{2C_0}{L} \varepsilon_R \tag{2}$$

$$\varepsilon(t) = -\frac{2C_0}{L} \int_0^t \varepsilon_R dt \tag{3}$$

In the above equations, A_0 and A are the cross-sections of the two bars and the specimen, respectively, L is the length of the specimen, C_0 is the bar wave speed, E_0 is the elastic modulus of the bars and the subscripts I, R and T denote incident, reflected and transmitted values, respectively. Once the engineering stresses (σ_{eng}) and strains (ε_{eng}) were obtained, constant volume approximation was invoked to obtain the corresponding true stress (σ_{true}) and true strain (ε_{true}) using the following equations:

$$\varepsilon_{true} = -\log(1 - \varepsilon_{eng}) \tag{4}$$

$$\sigma_{true} = \sigma_{eng}(1 - \varepsilon_{eng}) \tag{5}$$

4. Quasi-static tests

Compression tests on SF and IPC samples were conducted under static loading conditions. The microballoon volume fractions (V_f) of 10%, 20%, 30% and 40% were incorporated in both SF and IPC, and the effect was examined.

4.1. Syntactic foam

The compressive true stress vs. true strain responses for four types of syntactic foams (SF) (10, 20, 30 and 40% V_f) are shown in Fig. 3. These responses show three distinct stages of deformation typical of structural foams. An initial linear elastic region is followed by a distinct drop in stress with increasing strain after yielding. (This softening response is attributed to the one seen for neat epoxy sample tested under identical static loading conditions, discussed in Appendix A) The softening response is then followed by a region of nearly constant stress with increasing strain. In this plateau region microballoons within the SF fail progressively. Further increase in load causes densification (signified by an increasing stress) as microballoons collapse completely. These are consistent with similar observations made in a few earlier works [20–22] for different SF systems. As seen in Fig. 3, the stress–strain responses of syntactic foam samples of all four volume fractions follow a similar trend. It is also evident that the compressive strength decreases with increasing volume fraction of microballoons in the SF. The 10% V_f samples (SF-10) have a compressive strength of 63.2 MPa, whereas

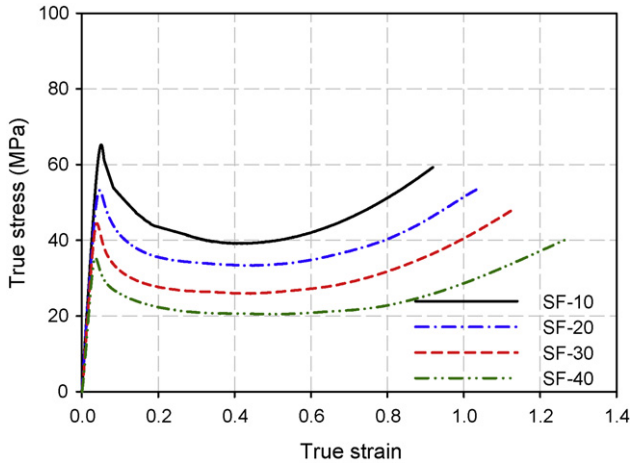

Fig. 3. Effect of microballoon volume fraction on quasi-static compression response of syntactic foam (SF) samples.

the SF-40 samples have only 34.4 MPa, a 45% decrease. (The elastic modulus values also show a decreasing trend with increasing microballoon volume fraction. The SF-10 samples have an elastic modulus of ~1600 MPa and the SF-40 samples, ~1260 MPa, which is a 21% decrease.) The true strain corresponding to the initial maximum stress are 4.5%, 4.0%, 3.3% and 3.1% for the SF-10, SF-20, SF-30 and SF-40 samples, respectively.

The plateau stress values of SF samples in the order of increasing volume fractions are approximately 40 MPa, 33.5 MPa, 26 MPa and 20.6 MPa. This trend of decreasing plateau stress with increasing microballoon volume fraction is also consistent with those predicted by Kim and Plubrai [21]. Furthermore, as the volume fraction of microballoons increase in SF, the densification strain also increases monotonically, from ~50% true strain for 10% V_f to ~75% true strain for 40% V_f. The deformed samples were sectioned and examined in a scanning electron microscope. Fig. 4 shows micrographs of deformed SF-30 samples corresponding to 14% (Fig. 4(a)) and 58% (Fig. 4(b)) strains. The onset of microballoon failure is evident in Fig. 4(a). Fig. 4(b) shows the microballoons to be almost completely crushed and flattened, which explains the densification or the increase in stress with increase in strain after ~50% strain. Furthermore, compression of the matrix and crushing of microballoons is uniform in the entire field of view. The direction of load in the micrographs is along the vertical axis, but a skew in the direction of the fractured microballoons is seen in Fig. 4(a) suggesting a tendency for shear failure, consistent with some of the previous works [20–22] as well.

4.2. IPC

The IPC foam samples used for quasi-static tests also had the same dimensions as the SF samples. The results for four different IPC samples with different volume fraction of microballoons in SF are shown in Fig. 5. The IPC foams respond in a way similar to SF samples (Fig. 3). There is an initial linear elastic region, followed by yielding and softening signifying the onset of nonlinearity. The softening is then followed by regions of plateau stress and densification. In the case of IPC, however, the onset of nonlinearity is also affected by progressive bending of the aluminum ligaments which in turn cause the crushing of the microballoons in between the ligaments (Fig. 6). The plateau region for IPC foam is relatively narrow when compared to the one for the corresponding syntactic foam. That is, densification starts at a relatively lower strain in IPC.

The elastic modulus for 10%, 20%, 30% and 40% volume fraction IPC foam samples are 2354 MPa, 2123 MPa, 1852 MPa and 1702 MPa, respectively. The compressive strengths of the IPC samples in the increasing order of volume fraction are 81.0 MPa, 63.1 MPa, 51.5 MPa and 44.0 MPa. The plateau stresses for the samples show a similar trend as the compressive strengths, that is, samples with a lower V_f of microballoons have higher plateau stresses. The true plateau stress values for the 10%, 20%, 30% and 40% V_f samples are approximately 59 MPa, 50 MPa, 40 MPa and 31 MPa, respectively, which is a ~10 MPa increase in plateau stress value for

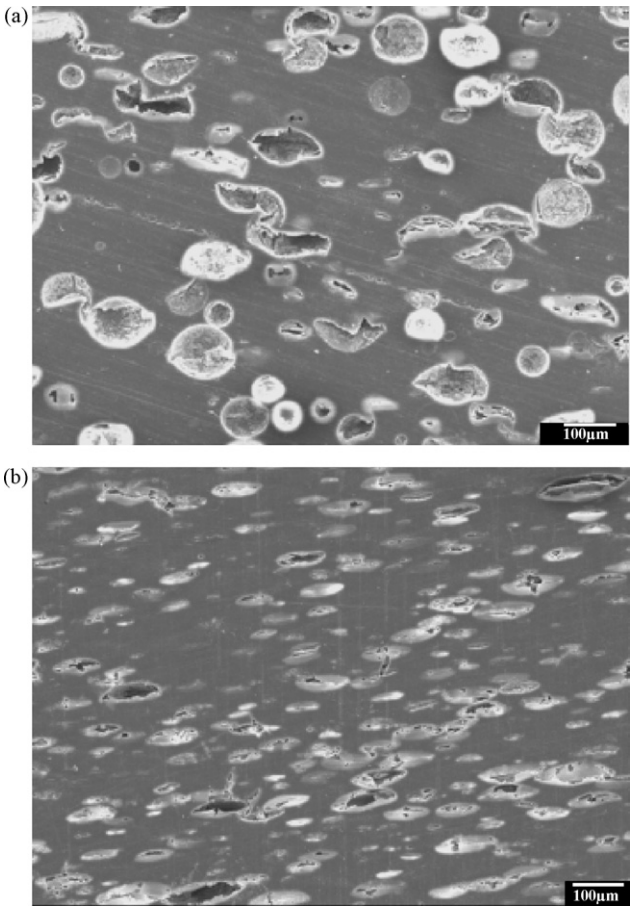

Fig. 4. SEM images of 30% *Vf* syntactic foam at (a) 14% strain and (b) 58% strain showing crushing of microballoons at various stages of static deformation. (The loading was in the vertical direction).

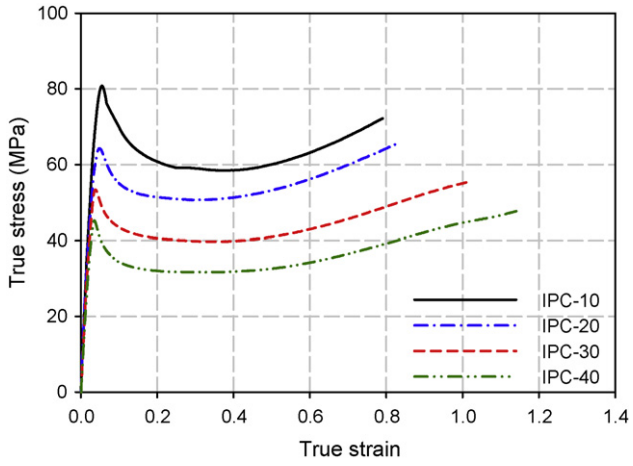

Fig. 5. Effect of microballoon volume fraction on quasi-static compression response of IPC foam samples.

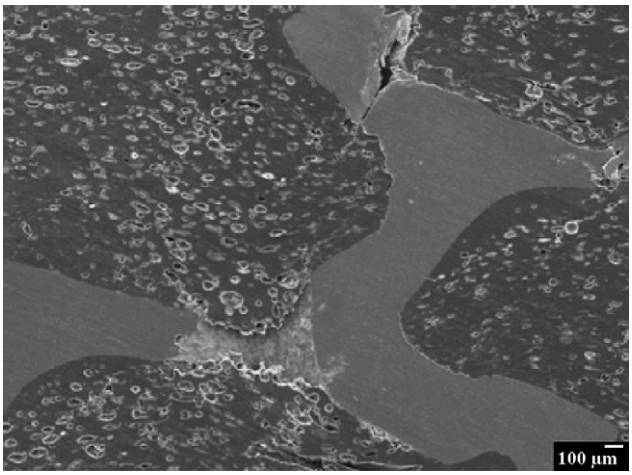

Fig. 6. SEM image of statically deformed IPC foam at 58% strain. (The loading was along the vertical direction).

10% decrease in V_f of microballoons. After yielding, the onset of densification also follows a uniform trend, wherein lower V_f samples have lower densification strain. The approximate true strain values which mark the onset of densification are in the 45–55% range.

Although the effect of microballoon volume fraction on IPC is similar to that for SF, when the elastic modulus of IPC is compared with that for the corresponding syntactic foam, it is evident that the IPC foams are stiffer. The relative increase in the elastic modulus values are 47%, 39%, 28% and 35% for 10%, 20%, 30% and 40% volume fraction of microballoons, respectively. The relative increases in the compressive strengths are in the range of 27–29%. A loss of densification strain relative to the corresponding SF counterpart is also evident when IPC results in Fig. 5 are compared with those of SF in Fig. 3. It is important to note that the increase in the plateau stress of IPC foams relative to the SF is substantially higher than that for unfilled aluminum network which is approximately in the range of 1.5–2.0 MPa [11]. A comparison of the plateau stress for SF and IPC foams (Figs. 3 and 5) of same volume fraction of microballoons show that the plateau stress increases by 10-20 MPa, substantially higher than that expected based on the value for unfilled aluminum preform (whose plateau stress is ~ 2 MPa [11]). This is attributed to the synergistic constraining effects between SF and aluminum network of an IPC enhancing the overall mechanical performance.

5. Dynamic tests

The SF and IPC samples with 10%, 20%, 30% and 40% microballoon volume fractions were tested at a strain rate of ~1500 per second using the split Hopkinson pressure bar. The maximum strain attained by a sample depends on the time period of the incident stress wave. This in turn depends on the length of the striker used [20]. Several striker lengths, 203 mm (8 in) to 406 mm (16 in.), were considered. In view of a relatively large expected strain to failure, the longest feasible striker length was considered. The incident pulse generated by the 406 mm long striker (impact velocity ~15 m/s) had a total time period of ~200 μs with a constant strain lasting over approximately 100μs as shown in the representative strain histories in Fig. 7 for SF and IPC samples with 30% volume fraction of microballoons. The maximum engineering strain experienced by the sample for this pulse was a little over 25%. So, conservatively, all analyses were based on a maximum specimen strain value of 25% and the stress–strain data once the stress pulse started to drop-off was not considered in the analysis. The repeatability of the set up was evaluated by comparing the stress–strain curves of multiple samples. Fig. 8 shows the stress–strain responses

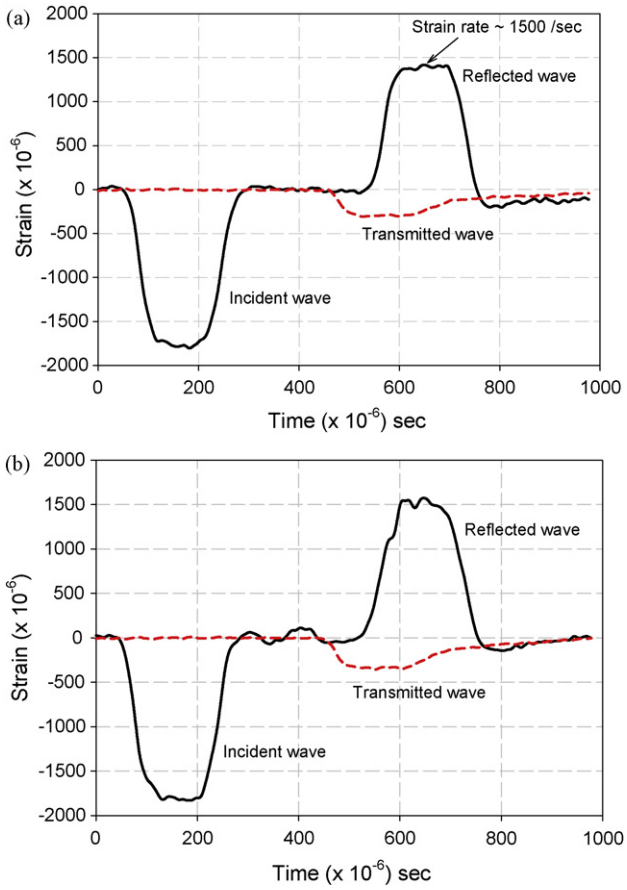

Fig. 7. Representative SHPB strain histories for (a) syntactic foam sample with 30% microballoon volume fraction and (b) IPC foam sample with 30% microballoon volume fraction.

of four 30% volume fraction SF samples obtained using a 203 mm striker producing a maximum engineering strain of approximately 15%. Good repeatability is evident from the figure.

5.1. Syntactic foam

The dynamic true stress - true strain responses of SF with four different volume fractions of microballoons obtained using

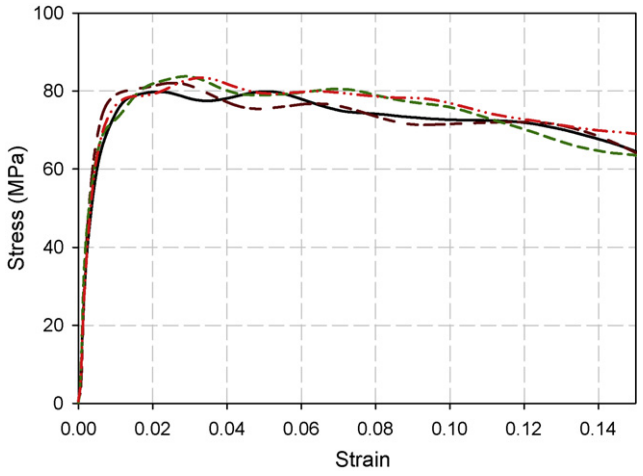

Fig. 8. Repeatability check done on four SF samples with 30% *Vf* of microballoons using a 203 mm striker at a strain rate of approximately 1500 s^{-1}. (Engineering stresses and strains are plotted).

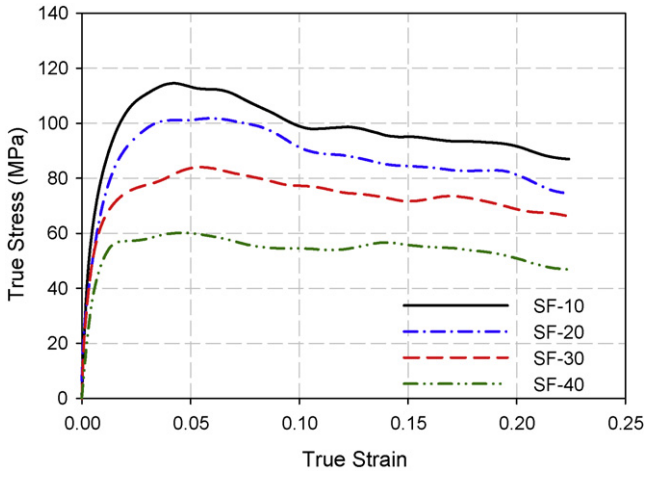

Fig. 9. Effect of microballoon volume fraction on dynamic stress–strain response of SF samples (Strain rate ~1500/s).

a 406 mm striker at a strain rate of ~1500 per second are shown in Fig. 9. The response of syntactic foam has two distinct phases. An initial linear elastic response followed by a monotonically decreasing stress region with increasing strain. As in the quasi-static cases, the compressive strengths of the samples decrease with increasing microballoon volume fraction. The compressive strengths of the 10%, 20%, 30% and 40% volume fraction samples were approximately 104 MPa, 80 MPa, 62 MPa and 50 MPa, respectively. The relative decrease in the compressive strengths for every 10% increase in the microballoon volume fraction is ~20%. A comparison of plots in Figs.3 and 9 show the influence of elevated loading rate on the stress–strain response of syntactic foam. Among the notable differences, dynamic loading clearly suppresses the distinct softening seen in quasi-static cases after the initial peak stress in all volume fractions (Fig. 3). Instead a more gradual softening is evident in Fig. 9. The tendency for the SF with lower volume fraction of microballoons (10% and 20%) to soften after attaining the maximum stress is somewhat more distinct than for the ones with higher volume fraction of microballoons (30% and 40%). These can be further attributed to the differences in neat epoxy response under static and dynamic loading conditions as described in Appendix A. After yielding, the stresses for SF with lower V_f of microballoons remain consistently higher than that for SF with higher V_f. The difference in stress values after yielding between specimens with different volume fraction of microballoons is approximately constant at all strains (within the observation window). The elastic responses under static and dynamic conditions also show differences. The measured elastic modulus for the four cases of syntactic foams is shown in Table 1. It should be noted that the dynamic elastic modulus values shown in Table 1 were obtained using ultrasonic pulse-echo measurements [24]. (This method was preferred over direct measurement from the stress–strain response due to weak stress equilibrium in the specimen during the initial stages (up to about 30 μs) of stress wave propagation in the specimen. The elastic moduli of the IPC are not reported here as the pulse-echo transducer could not be used effectively to determine wave speeds in IPC). The results indicate a higher elastic modulus under dynamic conditions when compared to the respective quasi-static counterparts (see, Table 2).

A backlit photograph of a deformed SF sample with 30% V_f of microballoons is shown in Fig. 10(a). The sample in this case was loaded along the vertical direction. A network of shear bands crisscrosses the entire sample and the bands are oriented at approximately ±45° to the loading direction. A micrograph of a 30% V_f specimen is shown in Fig. 10(b). Again, the direction of loading was along the vertical direction of the image. The cracks that appear in the image are skewed at an angle of approximately 45° to the direction application of the load. Interestingly, when compared to quasi-static counterparts (Fig.4(a) and (b)), microcracks are more distinctly localized, essentially connecting fractured microballoons along ±45° direction. In regions away from the crack, the microballoon footprints are circular suggesting very little deformation.

5.2. IPC

The IPC samples of four microballoon volume fractions *viz.* 10% (IPC-10), 20% (IPC-20), 30% (IPC-30) and 40% (IPC-40) were also tested and the results are shown in Fig. 11. The dynamic compression response of IPC foams followed trends similar to that of the corresponding syntactic foams. The response shows a linear region in the beginning, followed by a modest nonlinear response until a

Table 1
Dynamic properties of syntactic foam and IPC foam samples.

Designation	Microballoon volume fraction (%)	Density (kg/m^3)	Compressive strength (MPa)	Elastic modulus (MPa)
SF-10	10	995	104 ± 4	3460
SF-20	20	870	80 ± 3	3100
SF-30	30	796	62 ± 5	2700
SF-40	40	696	50 ± 3	2400
IPC-10	10	1169	120 ± 4	–
IPC-20	20	1044	100 ± 5	–
IPC-30	30	986	80 ± 6	–
IPC-40	40	862	60 ± 3	–

Table 2
Quasi-static properties of syntactic foam and IPC foam samples.

Designation	Microballoon volume fraction (%)	Density (kg/m^3)	Compressive strength (MPa)	Elastic modulus (MPa)
SF-10	10	995	63 ± 1.6	1600 ± 25
SF-20	20	870	52 ± 2.2	1530 ± 35
SF-30	30	796	42 ± 1.4	1448 ± 28
SF-40	40	696	34 ± 1.8	1261 ± 42
IPC-10	10	1169	81 ± 1.6	2354 ± 26
IPC-20	20	1044	63 ± 2.3	2123 ± 32
IPC-30	30	986	52 ± 3.6	1852 ± 27
IPC-40	40	862	44 ± 1.9	1702 ± 26

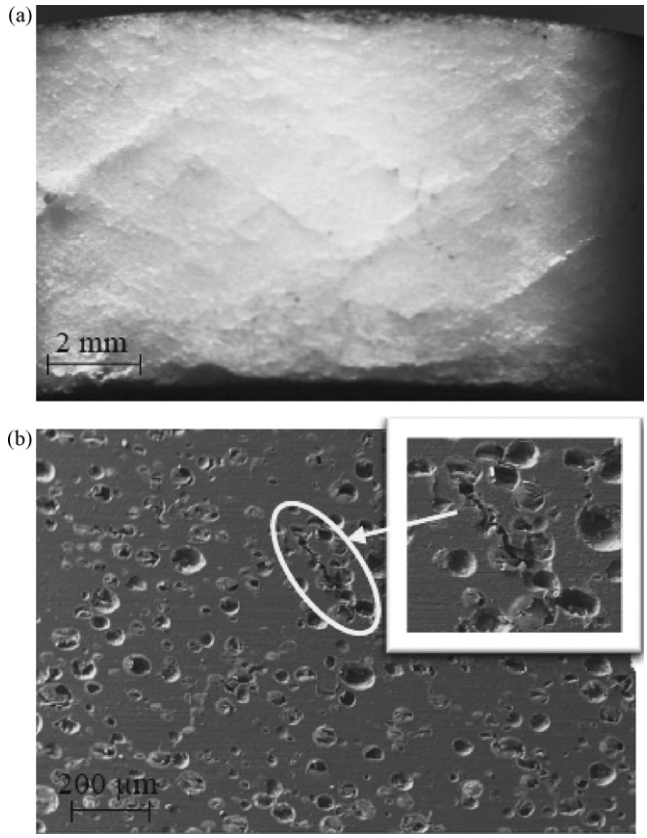

Fig. 10. (a) Side view of a dynamically deformed syntactic foam sample revealing a network of shear bands, (b) SEM image of cross-section of dynamically deformed syntactic foam; careful observation reveals crisscrossing shear failure planes. (The loading was along the vertical direction).

maximum stress is reached. Subsequently a monotonic reduction of stress with increasing strain is seen in the observation window up to 22% true strain. As in the case of SF samples, the yield strengths of IPC samples decrease with increasing volume fraction of microballoons. In the order of increasing microballoon V_f, the maximum stress values attained are approximately 120 MPa, 100 MPa, 80 MPa and 60 MPa. The percentage decrease in the compressive strength for the IPC-20 with respect to that of IPC-10 is 17%, and that of IPC-30 with respect to that of IPC-20 is 20%. The IPC-40 has a 25% decrease in compressive strength with respect to the IPC-30.

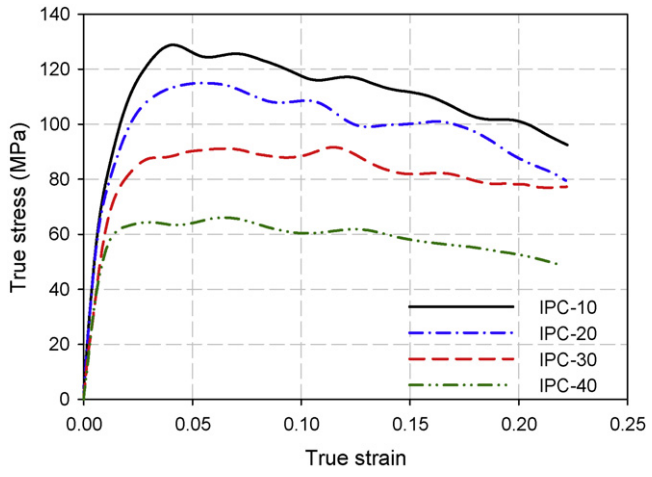

Fig. 11. Effect of microballoon volume fraction on dynamic stress–strain response of IPC foam samples (strain rate ~1500/s).

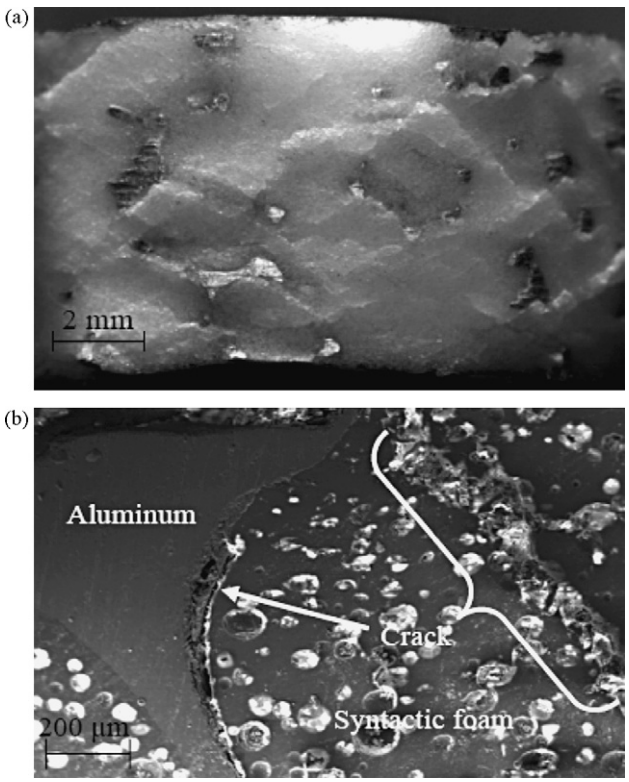

Fig. 12. (a) Side view of a dynamically deformed IPC foam sample revealing multiple shear bands and (b) SEM image of cross-section of dynamically deformed IPC foam. (The loading was along the vertical direction).

Fig. 12 shows a photograph and a micrograph of a deformed 40% V_f IPC. As in the SF samples, the photograph of the deformed sample in Fig. 12(a) clearly shows well-defined network of shear bands throughout the specimen. (The shear bands are slightly more pronounced and father apart due to the presence of the aluminum network.) The SEM image in Fig. 12(b) shows underlying microscopic failure mechanisms in the IPC. Two types of failures can be identified from this image. One is the formation of cracks in the syntactic foam (similar to the one seen for SF in Fig. 10(b)). The crack in Fig. 12(b) is again inclined at ±45° to the direction of load along the vertical direction of the image, which suggests that the failure occurred due to shear localization. However, shear bands here are interrupted by the metallic ligaments of the IPC. The other type of failure in IPC, which is absent in pure SF samples, is the debonding of the interfaces between the syntactic foam and the aluminum ligaments.

6. Energy absorption

An aspect of foams attractive for structural applications is energy absorption. A comparison of the energy absorbed per unit volume and per unit mass by the SF and the corresponding IPC samples under both static and dynamic loading conditions was made. The energy absorbed per unit volume (U) was evaluated by calculating the area under the true stress–true strain curve as,

$$U = \int_0^{\varepsilon} \sigma(\varepsilon) d\varepsilon \tag{6}$$

where $\sigma(\varepsilon)$ is the stress as a function of strain. The energy absorbed was evaluated up to a strain value of 22% for both static and dynamic cases as $U_{0.22}$ (Even though energy absorption can be computed up to 50–60% true strain under static loading conditions, for comparison with dynamic counterparts, it is limited to 22%). The energy

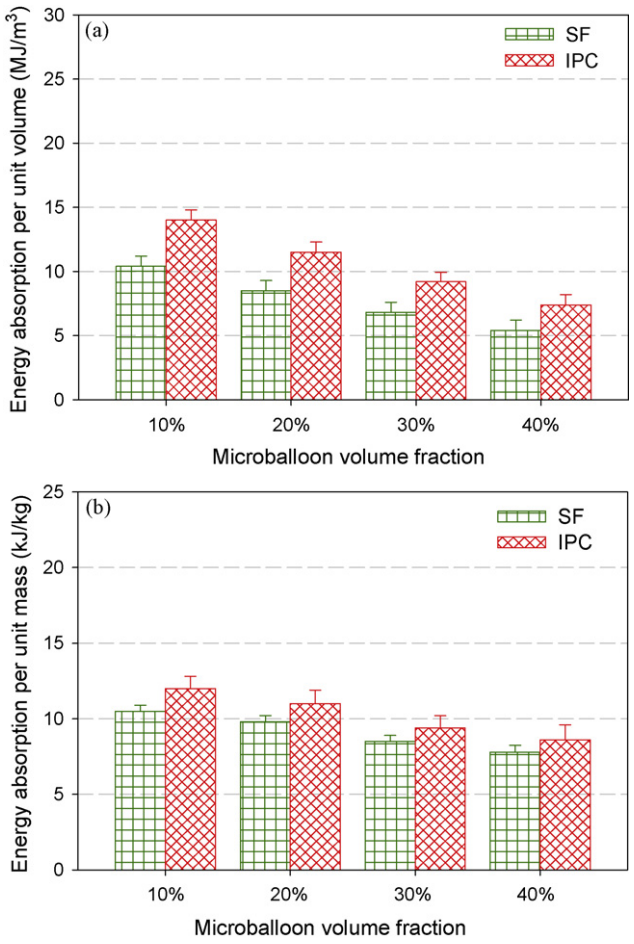

Fig. 13. Energy absorbed (a) per unit volume and (b) per unit mass by SF and IPC foam samples under quasi-static loading up to 22% true strain.

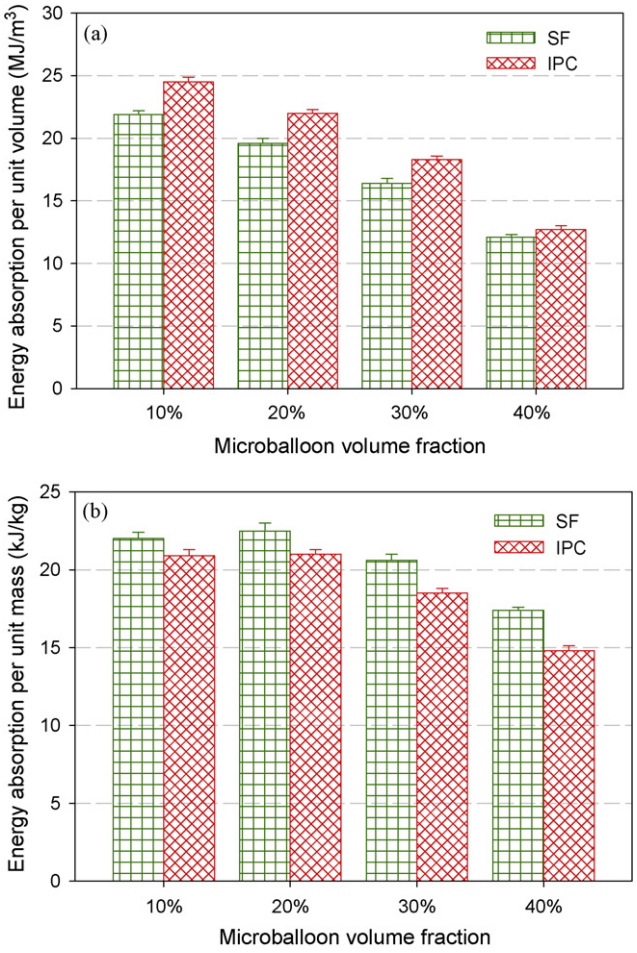

Fig. 14. Energy absorbed (a) per unit volume and (b) per unit mass by SF and IPC foam under dynamic loading up to 22% true strain.

absorption per unit mass was also evaluated by dividing the energy absorbed per unit volume by the density of the sample.

6.1. Quasi-static

The absorbed energy ($U_{0.22}$) evaluated from true stress–true strain graphs is plotted as histograms for all the cases in Fig. 13. As was the case for the compressive strength and the elastic modulus, the absorbed energies also show a decreasing trend with increasing volume fraction of microballoons. The energy absorbed per unit volume (Fig. 13(a)) by the SF samples of 10%, 20%, 30% and 40% microballoon V_f are 10.4 MJ/m^3, 8.5 MJ/m^3, 6.8 MJ/m^3 and 5.4 MJ/m^3, respectively. The relative decrease in $U_{0.22}$ for every 10% increase in microballoon V_f is 18–20%. The energy absorbed by the IPC samples is higher than that by the corresponding syntactic foam samples by 34–37%. The actual values are approximately 14.0 MJ/m^3, 11.5 MJ/m^3, 9.2 MJ/m^3 and 7.4 MJ/m^3 for 10%, 20%, 30% and 40% cases, respectively. The percentage decreases in $U_{0.22}$ for the IPC-20/IPC-10 pair, IPC-30/IPC-20 pair and the IPC-40/IPC-30 pair are approximately 20%, respectively. The energy absorption per unit mass are plotted in Fig. 13(b) and they also show a similar trend. The IPC samples have absorbed 12.0 kJ/kg, 11.0 kJ/kg, 9.4 kJ/kg and 8.6 kJ/kg which are higher when compared to the syntactic foams of corresponding volume fraction of microballoons, respectively. The percentage increase in the energy absorption per unit mass in the IPC foams with respect to the syntactic foams is approximately 10–14%.

6.2. Dynamic

The data on energy absorption, $U_{0.22}$, under dynamic loading conditions is shown in Fig. 14. The absorbed energies of SF and IPC foam samples under dynamic loading conditions are clearly higher than those observed under quasi-static loading conditions (Fig. 13). Energy absorbed per unit volume by SF-10, SF-20, SF-30 and SF-40 samples are 21.9 MJ/m^3, 19.6 MJ/m^3, 16.4 MJ/m^3 and 12.1 MJ/m^3, respectively and that by IPC-10, IPC-20, IPC-30 and IPC-40 samples are 24.5 MJ/m^3, 22.0 MJ/m^3, 18.3 MJ/m^3 and 12.7 MJ/m^3, respectively. These values are nearly double the respective quasi-static ones. The percentage reduction in $U_{0.22}$ per unit volume for the SF-20/SF-10 pair, SF-30/SF-20 pair and the SF-40/SF-30 pair are approximately 11%, 16% and 26% respectively. The percentage reduction in $U_{0.22}$ per unit volume for the IPC-20/IPC-10, IPC-30/IPC-20 pair and the IPC-40/IPC-30 pair are approximately 10%, 17% and 30%, respectively. The trend of the percentage reduction in the energy absorption per unit volume suggests that the rate of reduction in $U_{0.22}$ would be greater than the rate of increase of the microballoon volume fraction for dynamic loading. In the case of energy absorbed per unit mass though, the syntactic foam appears to perform better than the corresponding IPC foam under dynamic loading conditions. The energy absorbed per unit mass by the SF-10, SF-20, SF-30 and SF-40 samples are 22.0 kJ/kg, 22.5 kJ/kg, 20.6 kJ/kg and 17.4 kJ/kg, respectively and that by IPC-10, IPC-20, IPC-30 and IPC-40 samples are 20.9 kJ/kg, 21.0 kJ/kg, 18.5 kJ/kg and 14.8 kJ/kg, respectively. Again, these are nearly twice the respective quasi-static values. When compared

with the SF samples, the IPC samples had lower energy absorption per unit mass by 5%, 6.7%, 10.2% and 14.5%, respectively (It should be noted that the differences between 10% and 20% SF and between SF and IPC of the two volume fractions are relatively small with overlapping error bars. Hence, no claim regarding the trend between these two volume fractions is made). This is unlike the quasi-static loading cases which showed IPC samples to have higher specific energy absorption. Accordingly, *if energy absorption at a slight increase (~10%) in weight is acceptable for an application, IPC still outperforms SF even under dynamic conditions*. Another interesting observation is that the increasing trend of the energy absorption per unit mass with decreasing microballoon volume fraction gets reversed at a microballoon volume fraction of approximately 10%. Therefore, the 10% microballoon volume fraction could be used as a threshold in terms of absorbed energy per unit mass.

Another interesting outcome under dynamic loading conditions is strain recovery in SF and IPC foam samples. The final lengths of the deformed samples were measured after the experiments for both SF and IPC. Interestingly, for SF samples, the final measured lengths were more than that predicted by the SHPB equations following a 25% engineering strain. This suggests that the SF samples had partially recovered (sprung-back) after the loading pulse. Although the source/s of spring-back in SF is/are unclear at this point and would be of an interesting aspect to study in the future, this phenomenon was negligible in the IPC samples. Whatever that caused the spring-back in the SF, is probably overcome in the IPC by the aluminum ligaments. Once aluminum ligaments undergo plastic deformation, they prevent the SF from spring-back. This aspect of SF relative to IPC should have to be a consideration in an application if spring-back is a design factor. This issue was further examined optically by tracking the progression of deformation under static and dynamic loading conditions for both SF and IPC foams.

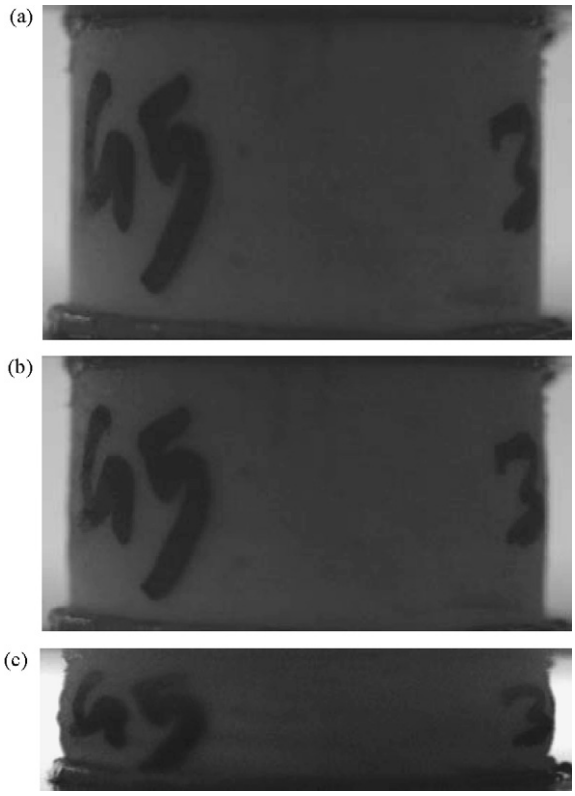

Fig. 15. Stages of quasi-static deformation of 20% syntactic foam at (a) 0%, (b) 10% and (c) 52% strain. (The loading was along the vertical direction).

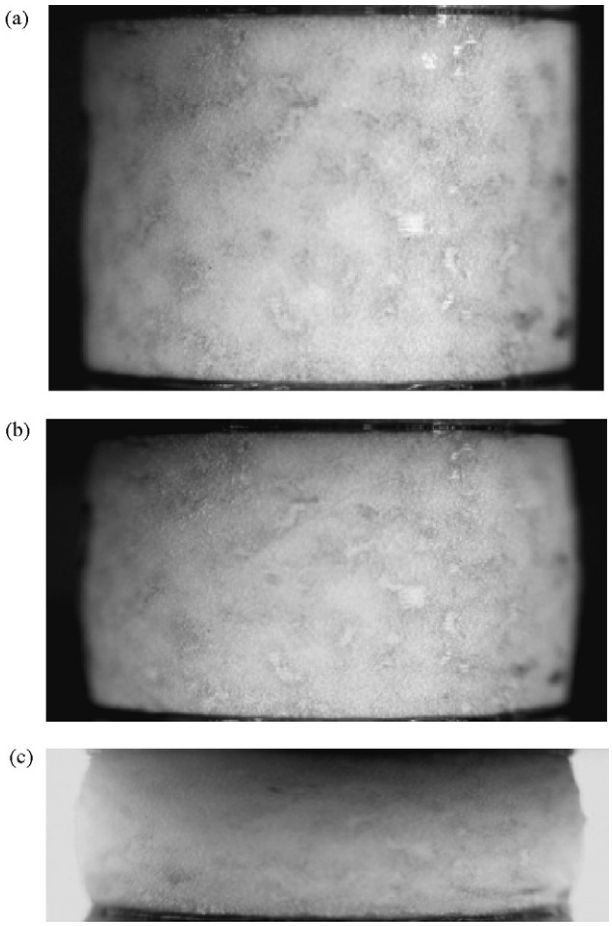

Fig. 16. Stages of quasi-static deformation of 30% IPC foam at (a) 0%, (b) 19% and (c) 48% strain. (The loading was along the vertical direction).

7. Failure progression

To understand the failure of SF and IPC foams including the above noted spring-back behavior in SF, real-time photography of progression of deformation during loading was carried out. This was also particularly important under dynamic loading conditions to assess progressive vs. steady-state deformation as stress waves propagate and deform the sample. Figs. 15 and 16 show three different stages in the quasi-static deformation process of syntactic foam (V_f = 20%) and IPC foam (V_f = 30%) samples. No significant barreling of the specimens is evident suggesting a uniaxial state of stress over the loading history. Upon unloading, neither SF nor IPC samples showed any measurable spring-back under quasi-static conditions.

The dynamic counterparts for SF with 30% V_f of microballoons is shown in Fig. 17. For a qualitative analysis of the overall specimen behavior during loading, two narrow (3 mm wide) diametrically opposite flat surfaces were machined on the foam samples and were printed with a line grating (pitch = 0.4 mm). The grating lines were first drafted using Solid Edge™ software and then printed on a decal paper. The printed grating lines on the decal paper were then transferred to the specimen surface.[2] A few selected photographs of the specimen with gratings recorded using digital high-speed photography (186,000 frames/s) are shown in Fig. 17. The image in

[2] Liu et al. have used circumferentially painted line markings [25] to photographically study the crushability and progression of compressive failure in rigidly confined low-density epoxy foams under quasi-static conditions.

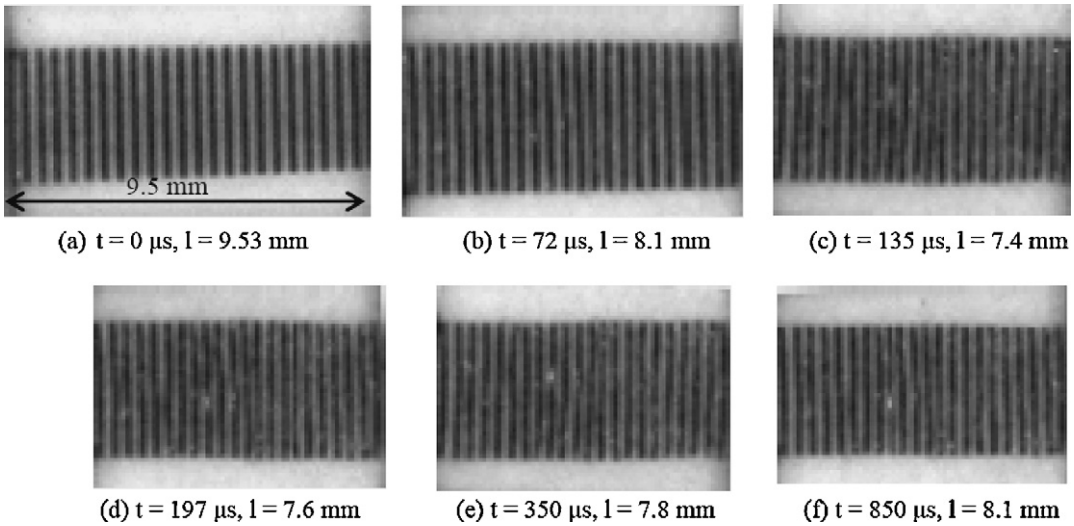

Fig. 17. Stages of dynamic deformation of SF-30. Images (a)–(c) correspond to the first loading pulse and (d)–(f) correspond to later time instants showing presence of spring-back. The pitch of the coarse grating lines is 0.4 mm. The sample was loaded in the horizontal direction; $t = 0$ corresponds to the time when deformation begins.

Fig. 17(a) corresponds to the undeformed sample just before the onset of the loading pulse in SHPB. The subsequent images show the deformed samples at different time instants (t). It is evident from the deformed length (l) that there was continuous decrease in the sample length up to 135 μs. This time instant is also when the loading pulse starts to decay due to the finite striker length. That is, $t = 135$ μs marks the end of the constant strain-rate region of the loading pulse. The approximate strain at 135 μs calculated directly from the image is ~23% which is close to the obtained engineering strain of 22% using SHPB equations. Around 195 μs the sample starts to spring-back. At the 850th μs the sample has regained about 0.7 mm in length which is about 9.5% of the deformed length at the end of the loading pulse at 135 μs. In Fig. 17(d), (e) and (f) correspond to time instants after the end of the first incident stress wave and before the second incident stress wave. From the images shown in Fig. 17, due to the coarseness of the gratings used, shear bands seen on the specimen surface in Fig. 10(a) are not readily evident although a hint of these bands can be visualized in Fig. 17(c) and beyond. Much higher gratings densities and magnification are needed to achieve the necessary spatial and temporal resolutions in this regard. To contrast the response of SF with that of IPC, a similar optical observation using high-speed photography was carried out for an IPC sample also. A selection of corresponding real-time images is shown in Fig. 18. (Noticeably, the quality of the images in these experiments is not as good as the ones in Fig. 17 due to the presence of shiny aluminum ligaments in the IPC which perturb the overall light field making it difficult to image the specimen. Nevertheless, qualitative observations regarding the nature of deformation progression can be made.) The spring-back phenomenon seen in SF is nearly absent in IPC samples under stress wave loading as evident from Fig. 18(d), (e) and (f).

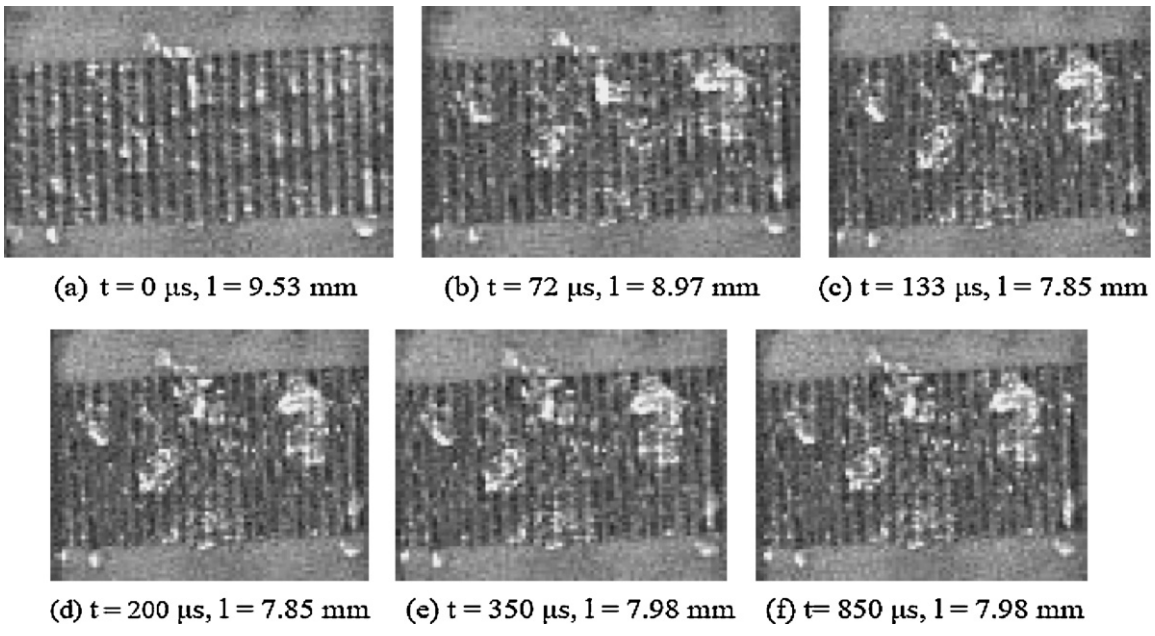

Fig. 18. Stages of dynamic deformation of IPC-30. Images (a)–(c) correspond to the first loading pulse and (d)–(f) correspond to later time instants showing absence of spring-back. The pitch of the coarse grating lines is 0.4 mm. The sample was loaded in the horizontal direction; $t = 0$ corresponds to the time when deformation begins.

8. Conclusions

The compression characteristics of a interpenetrating phase composite (IPC) foam was studied for static and dynamic applications. The IPC foam was made by infusing uncured epoxy-based closed-cell syntactic foam (SF) into open-cell aluminum preforms. Upon curing, an IPC structural foam with a 3D interconnectivity was formed.

The quasi-static and dynamic compression responses of IPC foams infused with SF containing 10–40% V_f of hollow glass microballoons were studied. For dynamic experiments a split Hopkinson pressure bar was employed and strain rates of ~1500/s were achieved. The responses of IPC foams were also evaluated relative to their pure SF counterparts. The failure progression in both types of samples was recorded using high-speed photography to examine the deformation processes. The micrographs were also used to explain the underlying failure mechanisms. The major conclusions of this work are as follows:

- The stress–strain responses under quasi-static conditions of SF and IPC foams show elastic, softening, plateau, and densification regimes. A monotonic increase in elastic modulus, yield stress, and plateau stress are evident as V_f of microballoons decrease. The IPC foams consistently have higher value of each of these characteristics relative to the corresponding SF.
- The plateau stresses for IPC foams are greater than the sum of the plateau stresses of the corresponding SF and unfilled aluminum preform/scaffold. This is attributed to the prevalence of synergistic mechanical constraint between the scaffold and SF phases of the 3D interpenetrating microstructure.
- The crushing of microballoons is relatively uniform in both SF and IPC samples under static conditions. Interfacial debonding is an additional failure mechanism seen in IPC foams.
- Unlike static results, under dynamic conditions SF and IPC samples show a stress–strain response that has only two dominant regimes – a proportional loading zone up to a maximum stress, and a monotonically softening zone subsequently. The elastic modulus and maximum stress increase with decreasing V_f of microballoons under high-strain-rate loading. The values for IPC are again higher than those for SF under dynamic conditions. The dynamic maximum stress values are also higher for both SF and IPC relative to the quasi-static ones.
- The energy absorbed, $U_{0.22}$, (up to 22% true strain) for SF and IPC samples show that IPC absorbs ~35% higher energy per unit volume than the corresponding SF under quasi-static conditions. The dynamic values of $U_{0.22}$ are nearly twice the corresponding static values for both IPC and SF samples. The energy absorbed per unit volume by the IPC under dynamic conditions is about ~10% higher than the SF counterparts. The energy absorbed per unit mass, however, favors SF under dynamic conditions.
- The failure of SF and IPC under dynamic conditions is dominated by the formation an extensive network of shear bands in SF. Also, the microballoons are not as uniformly crushed as in static cases.
- Unlike static results, the high-speed optical recordings of the deformation process reveal significant spring-back in SF whereas it is negligible in case of IPC. Also, the failure process is rather uniform in both SF and IPC and no evidence of spatially progressive failure is seen.

Acknowledgments

The authors gratefully acknowledge the support of the U.S. Army Research Office through grants W911NF-08-1-0285 and W911NF-06-1-0126 (DURIP) to HVT.

Appendix A.

A.1. SHPB calibration

The SHPB apparatus was first calibrated relative to the published results [26] in the literature for a low impedance material. The material tested was a commercially produced cast acrylic rod stock of 12.7 mm dia. Cylindrical samples of length 6.35 mm were machined from the stock and tested under conditions similar to that used for SF and IPC samples. The resulting true stress–strain diagram for a strain rate of approximately 1250/s is shown in Fig. A1. The results are compared with those reported in Ref. [26] for specimens made from cast acrylic sheet stock of identical specimen dimensions. The overall similarity in the stress–strain response with the reported ones is clearly evident. The minor deviations are attributed to differences in the specimen preparation, the stock material (sheet vs. rod) and strain rates used.

A.2. Neat epoxy compression response

The epoxy resin used for preparing SF and IPC foam samples were characterized under static and dynamic loading conditions as well. For completeness the corresponding data is reported in Fig. A2 up to 22% true strain. The quasi-static response of neat epoxy shows three distinct regions – initial linear elastic region, soften-

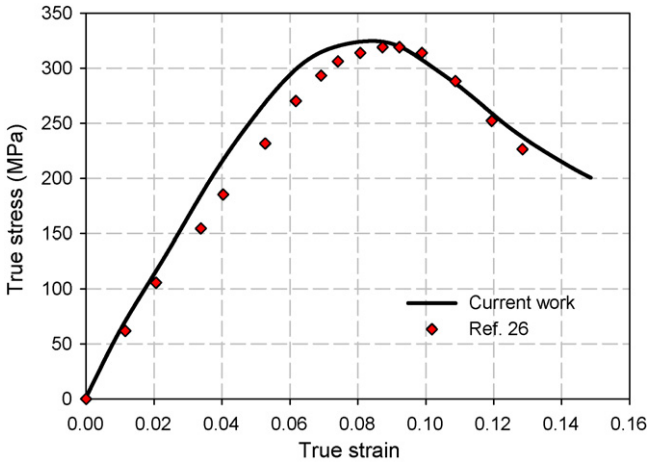

Fig. A1. True stress–strain response for cast acrylic; calibration of the SHPB apparatus.

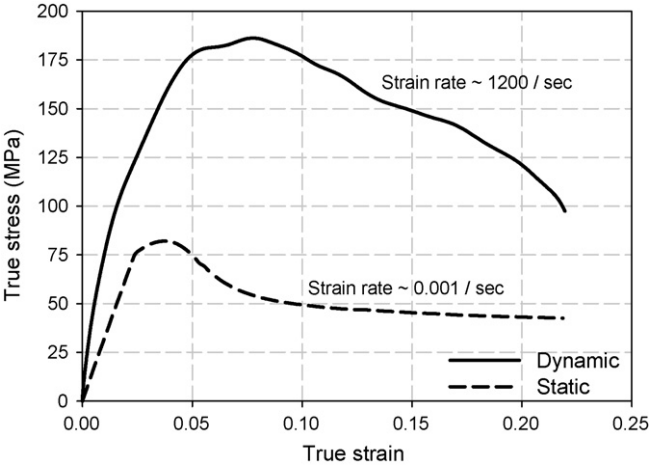

Fig. A2. Quasi-static and dynamic compressive responses of neat epoxy ("Epo-Thin") used in SF and IPC foams

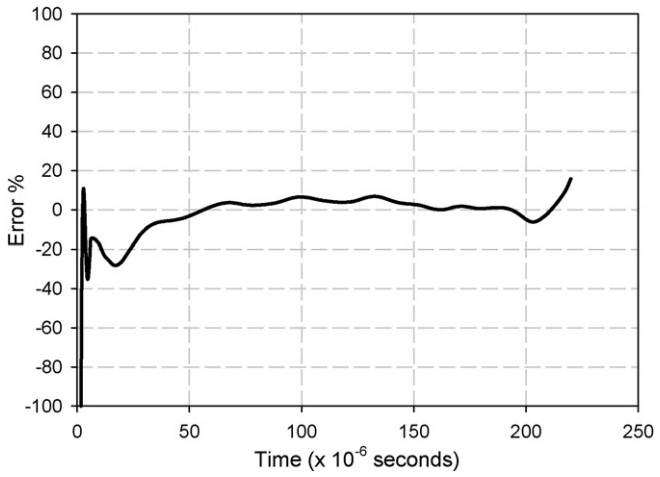

Fig. A3. An example to demonstrate dynamic stress equilibrium for SF-30. (The corresponding strain histories are shown in Fig. 8(a)).

ing region following yielding and a plateau stress region. A yield stress of approximately 80 ± 2 MPa is followed by a plateau stress of ~48 MPa up to 22% strain. At higher strains (not shown), a densification response is seen. (The sample continued to densify up to 70% strain). The dynamic response, on the other hand, has only two distinct regions. Following an initial linear response with a higher elastic modulus than the quasi-static counterpart, a maximum yield stress of $\sim 185 \pm 5$ MPa is attained by the neat epoxy sample. Subsequently, the sample shows a monotonic softening response until the stress pulse ends.

A.3. Dynamic stress equilibrium

The standard SHPB equations for strain rate, strain and stress in the specimen assume that the specimen was under dynamic stress equilibrium and at a constant strain rate during the loading. These two conditions were verified by plotting the percentage difference between the incident wave and the (reflected + transmitted) wave with respect to the incident wave. For the specimen to be under dynamic stress equilibrium, the stresses on the front and back ends or the specimen should be equal. That is, the incident wave should equal the sum of the reflected and the transmitted waves. From the graph (Fig. A3) it can be seen that the percentage difference is about 7% or less for most part of the loading pulse duration and that the dynamic equilibrium condition is satisfied quite well given the highly transient nature of the dynamic event. The equations [19] for SHPB reveal that the strain rate in the specimen is proportional to the reflected wave induced strain on the incident bar. The nearly constant strain region in the reflected wave (Fig. 7) suggests that the specimen was under a constant strain rate for about 125 μs during the dynamic loading event.

References

[1] D.R. Clark, Journal of the American Ceramic Society 75 (4) (1992) 739–759.
[2] H. Prielipp, M. Knechtel, N. Claussen, Materials Science and Engineering A 197 (1) (1995) 19–30.
[3] M.C. Breslin, J. Ringnalda, L. Xu, Materials Science and Engineering A 195 (1–2) (1995) 113–119.
[4] N.A. Travitzky, E.Y. Gutmanas, N. Claussen, Materials Letters 33 (1–2) (1997) 47–50.
[5] L.D. Wegner, L.J. Gibson, International Journal of Mechanical Sciences 42 (5) (2000) 925–942.
[6] L.D. Wegner, L.J. Gibson, International Journal of Mechanical Sciences 43 (4) (2001) 1061–1072.
[7] S. Skirl, M. Hoffman, K. Bowman, Acta Materalia 46 (7) (1998) 2493–2499.
[8] H. Mayer, M. Papakyriacou, Carbon 44 (9) (2006) 1801–1807.
[9] M.T. Tilbrook, R. Moon, M. Hoffman, Materials Science and Engineering A 393 (1–2) (2005) 170–178.
[10] T. Etter, J. Kuebler, T. Frey, Materials Science and Engineering A 386 (1–2) (2004) 61–67.
[11] R. Jhaver, H.V. Tippur, Materials Science and Engineering A (2009) 507–517.
[12] C. Hiel, D. Dittman, O. Ishai, Composites 24 (5) (1993) 447–450.
[13] F.A. Shutov, Advances in Polymer Science 73–74 (1986) 63–123.
[14] N. Gupta, S. Priya, R. Islam, et al., Ferroelectrics 345 (2006) 1–12.
[15] M.S. Kirugulige, R. Kitey, H.V. Tippur, Composites Science and Technology 65 (2005) 1052–1068.
[16] B. Song, W. Chen, Journal of Composite Materials 38 (11) (2004) 915–936.
[17] L.J. Gibson, Annual Review of Materials Science 30 (2000) 191–227.
[18] H. Kolsky, Proceedings of the Physical Society, Section B 62 (11) (1949) 676–700.
[19] M. Meyers, Dynamic Behavior of Materials, John Wiley & Sons, Inc., 1994, pp. 305-307.
[20] N. Gupta, Kishore, E. Woldsenbet, Journal of Materials Science 36 (18) (2001) 4485–4491.
[21] H.S. Kim, P. Plubrai, Composites Part A: Applied Science and Manufacturing 35 (9) (2004) 1009–1015.
[22] N. Gupta, E. Woldesenbet, Kishore, Journal of Materials Science 37 (15) (2002) 3199–3209.
[23] D.J. Frew, M.J. Forrestal, W. Chen, Experimental Mechanics 42 (1) (2002) 93–106.
[24] R.J. Butcher, C.E. Rousseau, H.V. Tippur, Acta Materialia 47 (1) (1998) 259–268.
[25] Q.L. Liu, G. Subhash, X.L. Gao, Journal of Porous Materials 12 (3) (2005) 233–248.
[26] A.D. Mulliken, M.C. Boyce, International Journal of Solids and Structures 43 (2006) 1331–1356.